

1    **High-level cognition is supported by information-rich but**  
2    **compressible brain activity patterns**

3                   Lucy L. W. Owen<sup>1,2</sup> and Jeremy R. Manning<sup>1,\*</sup>

4                   <sup>1</sup>Department of Psychological and Brain Sciences,  
5                   Dartmouth College, Hanover, NH

6                   <sup>2</sup>Carney Institute for Brain Sciences,  
7                   Brown University, Providence, RI

8                   \*Address correspondence to jeremy.r.manning@dartmouth.edu

9                   December 19, 2023

10                  **Abstract**

11                  We applied dimensionality reduction algorithms and pattern classifiers to functional neu-  
12                  roimaging data collected as participants listened to a story, temporally scrambled versions of  
13                  the story, or underwent a resting state scanning session. These experimental conditions were  
14                  intended to require different depths of processing and inspire different levels of cognitive en-  
15                  gagement. We considered two primary aspects of the data. First, we treated the maximum  
16                  achievable decoding accuracy across participants as an indicator of the “informativeness” of  
17                  the recorded patterns. Second, we treated the number of features (components) required to  
18                  achieve a threshold decoding accuracy as a proxy for the “compressibility” of the neural pat-  
19                  terns (where fewer components indicate greater compression). Overall, we found that the peak  
20                  decoding accuracy (achievable without restricting the numbers of features) was highest in the  
21                  intact (unscrambled) story listening condition. However, the number of features required to  
22                  achieve comparable classification accuracy was also lowest in the intact story listening con-  
23                  dition. Taken together, our work suggests that our brain networks flexibly reconfigure according  
24                  to ongoing task demands, and that the activity patterns associated with higher-order cogni-  
25                  tion and high engagement are both more informative and more compressible than the activity  
26                  patterns associated with lower-order tasks and lower levels of engagement.

27                  **Keywords:** information, compression, temporal decoding, dimensionality reduction, neu-  
28                  roimaging

29                  **Introduction**

30                  Large-scale networks, including the human brain, may be conceptualized as occupying one or  
31                  more positions along on a continuum. At one extreme, every node is fully independent from  
32                  every other node. At the other extreme, all nodes behave identically. Each extreme optimizes  
33                  key properties of how the network functions. When every node is independent, the network is

29 maximally *expressive*: if we define the network’s “state” as the activity pattern across its nodes, then  
30 every state is equally reachable by a network with fully independent nodes. On the other hand, a  
31 network of identically behaved nodes optimizes *robustness*: any subset of nodes may be removed  
32 from the network without any loss of function or expressive power, as long as any single node  
33 remains. Presumably, most natural systems tend to occupy positions between these extremes. We  
34 wondered: might the human brain reconfigure itself to be more flexible or more robust according  
35 to ongoing demands? In other words, might the brain reconfigure its connections or behaviors  
36 under different circumstances to change its position along this continuum?

37 Closely related to the above notions of expressiveness versus robustness are measures of  
38 how much *information* is contained in a given signal or pattern, and how *redundant* a signal  
39 is (Shannon, 1948). Formally, information is defined as the amount of uncertainty about a given  
40 variables’ outcomes (i.e., entropy), measured in *bits*, or the optimal number of yes/no questions  
41 needed to reduce uncertainty about the variable’s outcomes to zero. Highly complex systems with  
42 many degrees of freedom (i.e., high flexibility and expressiveness), are more information-rich than  
43 simpler or more constrained systems. The redundancy of a signal denotes the difference between  
44 how expressive the signal *could* be (i.e., proportional to the number of unique states or symbols  
45 used to transmit the signal) and the actual information rate (i.e., the entropy of each individual  
46 state or symbol). If a brain network’s nodes are fully independent, then the number of bits required  
47 to express a single activity pattern is proportional to the number of nodes. The network would  
48 also be minimally redundant, since the status of every node would be needed to fully express a  
49 single brain activity pattern. If a brain network’s nodes are fully coupled and identical, then the  
50 number of bits required to express a single activity pattern is proportional to the number of unique  
51 states or values any individual node can take on. Such a network would be highly redundant,  
52 since knowing any individual node’s state would be sufficient to recover the full-brain activity  
53 pattern. Highly redundant systems are also robust, since there is little total information loss due  
54 to removing any given observation.

55 We take as a given that brain activity is highly flexible: our brains can exhibit nearly infinite  
56 varieties of activity patterns. This flexibility implies that our brains’ activity patterns are highly  
57 information rich. However, brain activity patterns are also highly structured. For example,  
58 full-brain correlation matrices are stable within (Finn et al., 2017, 2015; Gratton et al., 2018) and

59 across (Cole et al., 2014; Glerean et al., 2012; Gratton et al., 2018; Yeo et al., 2011) individuals. This  
60 stability suggests that our brains' activity patterns are at least partially constrained, for example  
61 by anatomical, external, or internal factors. Constraints on brain activity that limit its flexibility  
62 decrease expressiveness (i.e., its information rate). However, constraints on brain activity also  
63 increase its robustness to noise (e.g., "missing" or corrupted signals may be partially recovered).  
64 For example, recent work has shown that full-brain activity patterns may be reliably recovered  
65 from only a relatively small number of implanted electrodes (Owen et al., 2020; Scangos et al.,  
66 2021). This robustness property suggests that the relevant signal (e.g., underlying factors that  
67 have some influence over brain activity patterns) are compressible.

68 To the extent that brain activity patterns contain rich task-relevant information, we should be  
69 able to use the activity patterns to accurately differentiate between different aspects of a task (e.g.,  
70 using pattern classifiers; Norman et al., 2006). For example, prior work has shown a direct  
71 correspondence between classification accuracy and the information content of a signal (Alvarez,  
72 2002). To the extent that brain activity patterns are compressible, we should be able to generate  
73 simplified (e.g., lower dimensional) representations of the data while still preserving the relevant  
74 or important aspects of the original signal. In general, information content and compressibility are  
75 related but are partially dissociable (Fig. 1). If a given signal (e.g., a representation of brain activity  
76 patterns) contains more information about ongoing cognitive processes, then the peak decoding  
77 accuracy should be high. And if the signal is compressible, a low-dimensional embedding of the  
78 signal will be similarly informative as the original signal (Fig. 1D).

79 Several recent studies suggest that the complexity of brain activity is task-dependent, whereby  
80 simpler tasks with lower cognitive demands are reflected by simpler and more compressible brain  
81 activity patterns, and more complex tasks with higher cognitive demands are reflected by more  
82 complex and less compressible brain activity patterns (Mack et al., 2020; Owen et al., 2021). These  
83 findings complement other work suggesting that functional connectivity (correlation) patterns are  
84 task-dependent (Cole et al., 2014; Finn et al., 2017; Owen et al., 2020), although see Gratton et  
85 al. (2018). Higher-order cognitive processing of a common stimulus also appears to drive more  
86 stereotyped task-related activity and functional connectivity across individuals (Hasson et al.,  
87 2008; Lerner et al., 2011; Simony & Chang, 2020; Simony et al., 2016).

88 The above studies are consistent with two potential descriptions of how cognitive processes are

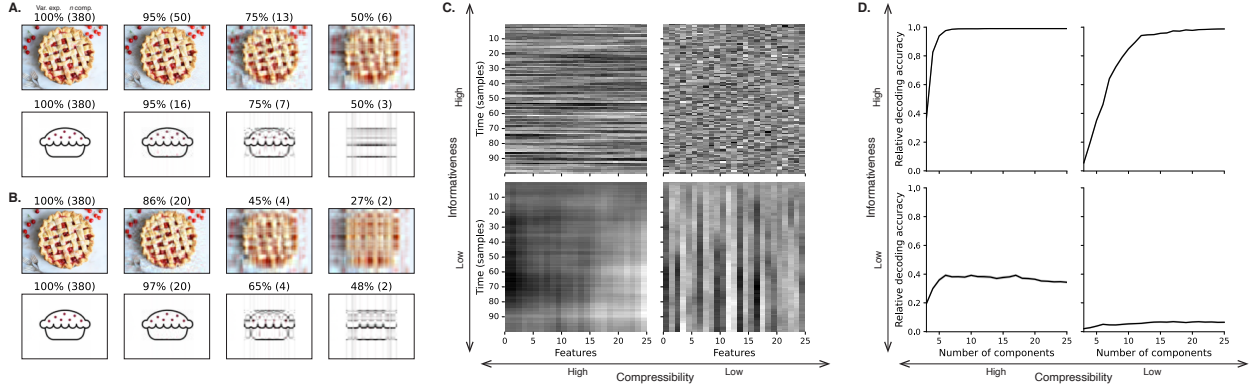


**Figure 1: Information content and compressibility.** **A. Variance explained for two images.** Consider two example images: a photograph and simple drawing. The images have the same resolutions, but their content is very different. The photograph is more information rich: when we compare the original photograph and drawing (leftmost column), we can see that the photograph captures much more detail. We can also apply principal components analysis to the images, treating the rows of the images as “observations.” Across columns, we identified the numbers of components required to explain 100%, 95%, 75%, or 50% of the cumulative variance in each image (the 100% columns denote the original images). The numbers of components are indicated in parentheses, and the resulting “compressed” images are displayed. This analysis reveals that the drawing is more compressible: just 16 components can explain 95% of the variance in the drawing, whereas 50 components are required to explain 95% of the variance in the photograph. **B. Representing two images with different numbers of components.** Using the same principal component decompositions as in Panel A, we computed the cumulative proportion of variance explained with 380 (original images), 20, 4, or 2 components. This analysis provides another way of characterizing the compressibility of each image by showing that the same number of components can explain more variance in the drawing than in the photograph. **C. Template data from four synthetic datasets.** We constructed four synthetic datasets, each comprising 25 features (columns) observed across 100 samples (rows) from each of 10 simulated “participants.” The datasets were constructed to contain different levels of informativeness and compressibility (see *Synthetic data*). **D. Decoding accuracy by number of components.** For each synthetic dataset, we trained across-participant classifiers to decode timepoint labels. Each panel displays the decoding accuracy as a function of the number of components used to represent the data. Error ribbons denote bootstrap-estimated 95% confidence intervals.

89 reflected in brain activity patterns. One possibility is that the information rate of brain activity in-  
90 creases during more complex or higher-level cognitive processing. If so, then the ability to reliably  
91 decode cognitive states from brain activity patterns should improve with task complexity or with  
92 the level (or “depth”) of cognitive processing. A second possibility is that the compressibility of  
93 brain activity patterns increases during more complex or higher-level cognitive processing. If so,  
94 then individual features of brain recordings, or compressed representations of brain recordings,  
95 should carry more information during complex or high-level (versus simple or low-level) cognitive  
96 tasks.

97 We used a previously collected neuroimaging dataset to estimate the extent to which each of  
98 these two possibilities might hold. The dataset we examined comprised functional magnetic reso-  
99 nance imaging (fMRI) data collected as participants listened to an audio recording of a 10-minute  
100 story, temporally scrambled recordings of the story, or underwent a resting state scan (Simony  
101 et al., 2016). Each of these experimental conditions evokes different depths of cognitive process-  
102 ing (Hasson et al., 2008; Lerner et al., 2011; Owen et al., 2021; Simony et al., 2016). We used  
103 across-participant classifiers to decode listening times in each condition, as a proxy for how “infor-  
104 mative” the task-specific activity patterns were (Simony & Chang, 2020). We also used principle  
105 components analysis to generate lower-dimensional representations of the activity patterns. We  
106 then repeated the classification analyses after preserving different numbers of components and  
107 examined how classification accuracy changed across the different experimental conditions.

## 108 Results

109 We sought to understand whether higher-level cognition is reflected by more reliable and in-  
110 formative brain activity patterns, and how compressibility of brain activity patterns relates to  
111 cognitive complexity. We developed a computational framework for systematically assessing the  
112 informativeness and compressibility of brain activity patterns recorded under different cognitive  
113 circumstances. We used across-participant decoding accuracy (see *Forward inference and decoding*  
114 *accuracy*) as a proxy for informativeness. To estimate the compressibility of the brain patterns, we  
115 used group principal components analysis (PCA) to project the brain patterns into  $k$ -dimensional  
116 spaces, for different values of  $k$  (see *Hierarchical Topographic Factor Analysis (HTFA)* and *Principal*

117 components analysis (PCA)). For more compressible brain patterns, decoding accuracy should be  
118 more robust to small values of  $k$ .

119 We analyzed a dataset collected by Simony et al. (2016) that comprised four experimental con-  
120 ditions. These conditions exposed participants to stimuli that systematically varied in cognitive  
121 engagement. In the *intact* experimental condition, participants listened to an audio recording of a  
122 10-minute Moth Radio Hour story, *Pie Man*, by Jim O’Grady. In the *paragraph*-scrambled experi-  
123 mental condition, participants listened to a temporally scrambled version of the story, where the  
124 paragraphs occurred out of order, but where the same set of paragraphs was presented over the  
125 entire listening interval. All participants in this condition experienced the scrambled paragraphs  
126 in the same order. In the *word*-scrambled experimental condition, participants listened to a tem-  
127 porally scrambled version of the story, where the words occurred in a random order. Again, all  
128 participants in this condition experienced the scrambled words in the same order. Finally, in the  
129 *rest* experimental condition, participants lay in the scanner with no overt stimulus, while keeping  
130 their eyes open and blinking as needed. This public dataset provided a convenient means for  
131 testing our hypothesis that different levels of cognitive processing and engagement affect how  
132 informative and compressible the associated brain patterns are.

133 To evaluate the relation between informativeness and compressibility for brain activity from  
134 each experimental condition, we trained a series of across-participant temporal decoders on com-  
135 pressed representations of the data. Figure 2A displays the decoding accuracy as a function  
136 of the number of principal components used to represent the data (also see Fig. S1). Several  
137 patterns were revealed by the analysis. First, in general (i.e., across experimental conditions),  
138 decoding accuracy tends to improve as the number of components are increased. However, de-  
139 coding accuracy peaked at higher levels for experimental conditions that exposed participants  
140 to cognitively richer stimuli (Fig. 2D). The peak decoding accuracy was highest for the “intact”  
141 condition (versus paragraph:  $t(99) = 35.205, p < 0.001$ ; versus word:  $t(99) = 43.172, p < 0.001$ );  
142 versus rest:  $t(99) = 81.361, p < 0.001$ ), next highest for the “paragraph” condition (versus word:  
143  $t(99) = 6.243, p < 0.001$ ; versus rest:  $t(99) = 50.748, p < 0.001$ ), and next highest for the “word”  
144 condition (versus rest:  $t(99) = 48.791, p < 0.001$ ). This ordering implies that cognitively richer  
145 conditions evoke more stable brain activity patterns across people.

146 The cognitively richer conditions also displayed steeper initial slopes. For example, the intact

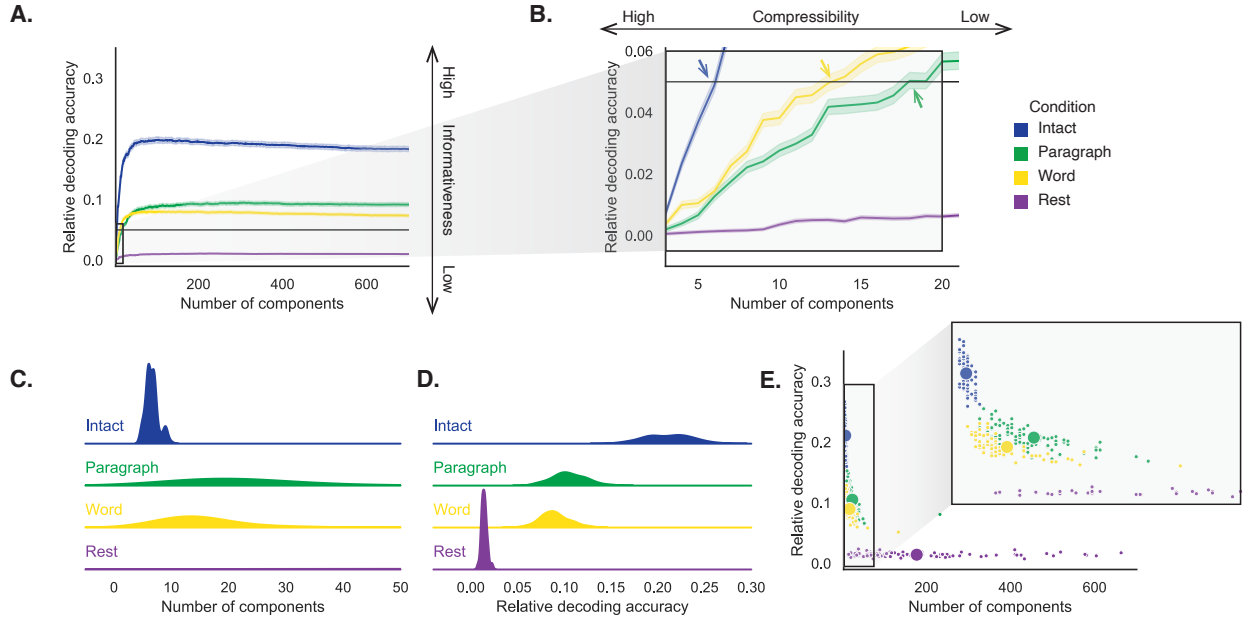


**Figure 2: Decoding accuracy and compression.** **A. Decoding accuracy by number of components.** Ribbons of each color display cross-validated decoding performance for each condition (intact, paragraph, word, and rest), as a function of the number of components (features) used to represent the data. For each condition, decoding accuracy has been normalized by subtracting expected “chance” decoding performance (estimated as  $\frac{1}{T}$ , where  $T$  is the number of timepoints in the given condition). This normalization was intended to enable fairer comparisons across conditions; a relative decoding accuracy of 0.0 denotes “chance” performance. The horizontal black line denotes 5% decoding accuracy (used as a reference in Panel B). **B. Numbers of components required to reach a fixed decoding accuracy threshold, by condition.** The panel displays a zoomed-in view of the inset in Panel A. Intersections between each condition’s decoding accuracy curve and the 5% decoding accuracy reference line are marked by arrows. All error ribbons in Panels A and B denote bootstrap-estimated 95% confidence intervals. **C. Estimating “compressibility” for each condition.** The density plots display the numbers of components required to reach at least 5% (corrected) decoding accuracy, across all cross validation runs. For the “rest” condition, where decoding accuracy never reached 5% accuracy, we display the distribution of the numbers of components required to achieve the peak decoding accuracy in each fold. (This distribution is nearly flat, as also illustrated in Panel E.) **D. Estimating “informativeness” for each condition.** The density plots display the peak (corrected) decoding accuracies achieved in each condition, across all cross validation runs. **E. Informativeness versus compressibility.** Each dot displays the minimum number of components required to achieve at least 5% corrected decoding accuracy ( $x$ -coordinate; for the rest condition the numbers of components are estimated using the peak decoding accuracies as in Panel C) and the peak (corrected) decoding accuracy ( $y$ -coordinate). The smaller dots correspond to individual cross validation runs and the larger dots display the averages across runs. The inset displays a zoomed-in view of the indicated region in the main panel.

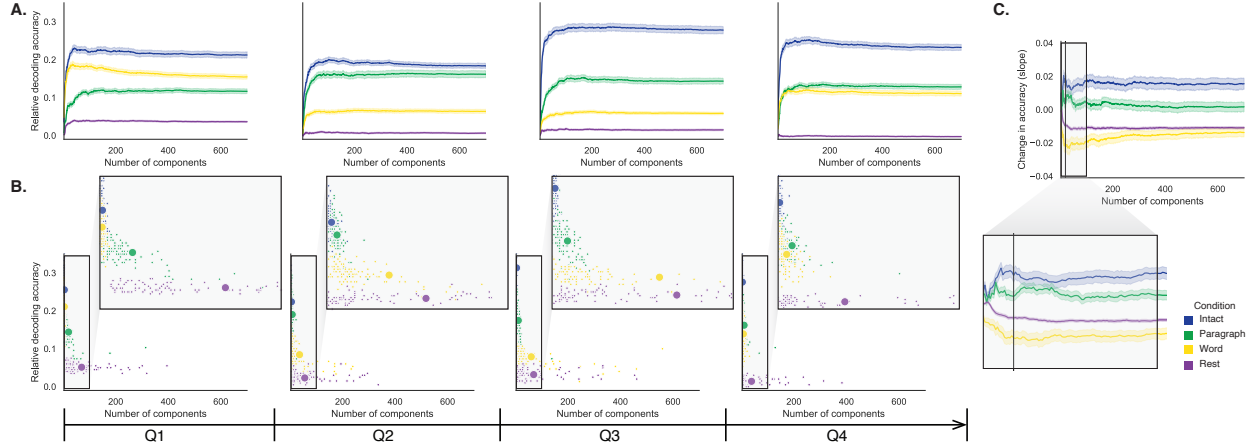


**Figure 3: Changes in decoding accuracy and compression over time.** **A. Decoding accuracy by number of components, by story segment.** Each family of curves is plotted in the same format as Figure 2A but reflects data only from one quarter of the dataset. **B. Informativeness versus compressibility by condition and segment.** Each scatter plot is in the same format as Figure 2E, but reflects data only from one quarter of the dataset. **C. Change in decoding accuracy over time, by number of components.** For each number of components ( $x$ -axis) and condition (color), we fit a regression line to the decoding accuracies obtained for the first, second, third, and fourth quarters of the dataset (corresponding to the columns of Panels A and B). The  $y$ -axis denotes the slopes of the regression lines. The black vertical line marks  $k = 20$  components, as referenced in the main text. All error ribbons denote bootstrap-estimated 95% confidence intervals.

147 condition decoders reached an arbitrarily chosen threshold of 5% accuracy using fewer components  
 148 than the paragraph condition decoders ( $t(99) = -7.429, p < 0.001$ ) or word condition decoders  
 149 ( $t(99) = -7.300, p < 0.001$ ), and decoding accuracy never exceeded 5% for the rest condition. This  
 150 suggests that brain activity patterns evoked by cognitively richer conditions are more compressible,  
 151 such that representing the data using the same number of principal components provides more  
 152 information to the temporal decoders (Figs. 2B, C). Taken together, as shown in Figure 2E, we  
 153 found that brain activity patterns evoked by cognitively richer conditions tended to be both more  
 154 informative (i.e., associated with higher peak decoding accuracies) *and* more compressible (i.e.,  
 155 requiring fewer components to achieve the 5% accuracy threshold).

156 If informativeness (to the temporal decoders) and compressibility vary with the cognitive  
 157 richness of the stimulus, might these measures also vary over time *within* a given condition? For  
 158 example, participants in the intact condition might process the ongoing story more deeply later  
 159 on in the story (compared with earlier in the story) given the additional narrative background  
 160 and context they had been exposed to by that point. To examine this possibility, we divided each

condition into four successive time segments. We computed decoding curves (Fig. 3A) and the numbers of components required to achieve 5% decoding accuracy (Fig. 3B) for each segment and condition. We found that, in the two most cognitively rich conditions (intact and paragraph), both decoding accuracy and compressibility, as reflected by the change in decoding curves, increased with listening time (e.g., at the annotated reference point of  $k = 20$  components in Fig. 3C: intact:  $t(99) = 7.915, p < 0.001$ ; paragraph:  $t(99) = 2.354, p = 0.021$ ). These changes may reflect an increase in comprehension or depth of processing with listening time. In contrast, the decoding accuracy and compressibility decreased with listening time in the word condition ( $t(99) = -10.747, p < 0.001$ ) and rest condition ( $t(99) = -22.081, p < 0.001$ ). This might reflect the depletion of attentional resources in the less-engaging word and rest conditions.

We also wondered how informativeness and compressibility in the different experimental conditions might vary across brain networks. We used a network parcellation identified by Yeo et al. (2011) to segment the brain into seven distinct networks. The networks can be sorted (roughly) in order from lower-level to higher-level cortex as follows (Figs. 4A–C): visual, somatomotor, dorsal attention, ventral attention, limbic, frontoparietal, and default mode. Next, we computed decoding curves separately for the activity patterns within each network and identified each network's inflection point, for each experimental condition. Moving from low-order networks to higher-order networks, we found that decoding accuracy tended to increase, particularly in the higher-level experimental conditions (Fig. 4D, E). This suggests that higher-order networks may carry more content-relevant or stimulus-driven "information." We found no clear trends in the proportions of components required to achieve 5% decoding accuracy across networks or conditions (Fig. 4F).

In addition to examining different networks in isolation, we wondered about the general structure of the full-brain (i.e., potentially multi-network) activity patterns reflected by different principal components across different experimental conditions. As shown in Figure 5, we used Neurosynth (Rubin et al., 2017) to identify, for each component, the associations with each of 80 themes (see *Reverse inference*). In general, the first principal components across all of the experimental conditions tended to weight most heavily on themes related to cognitive control, memory, language processing, attention, and perception. Other components appeared to vary more across conditions.

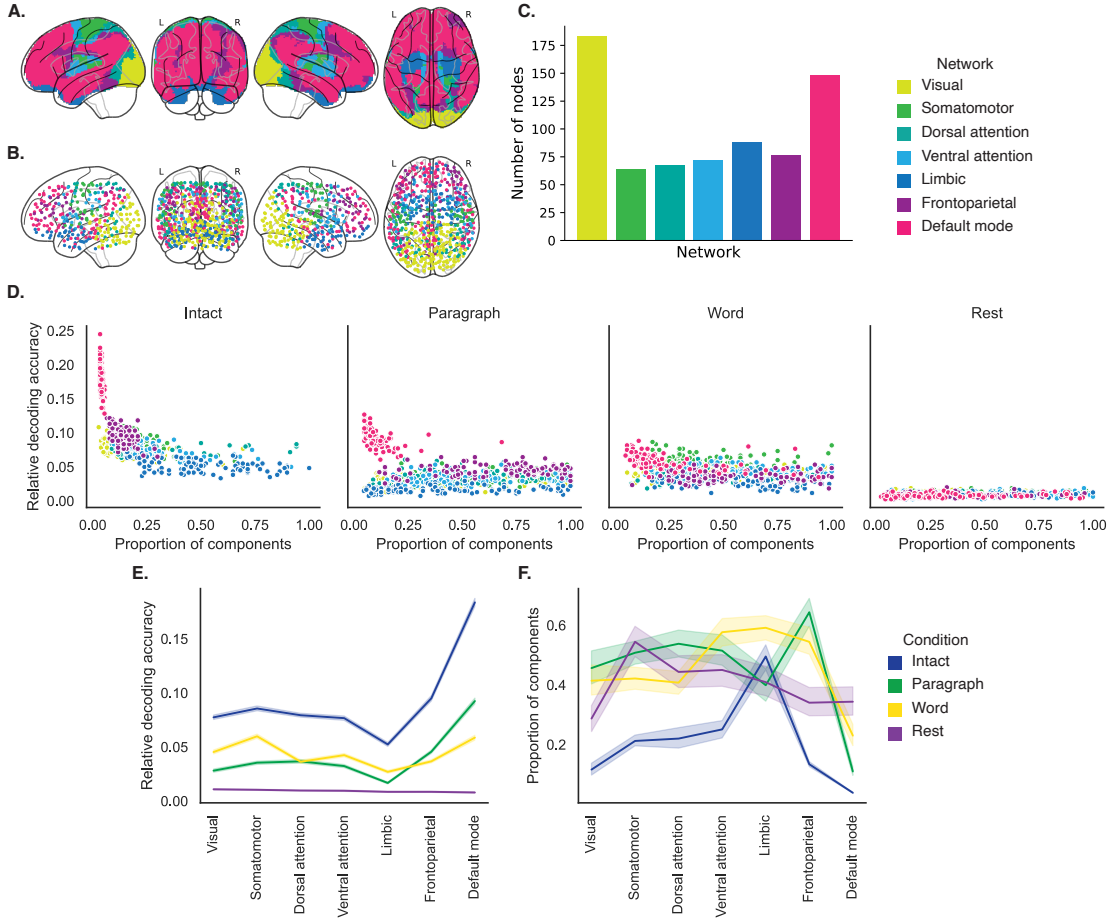


**Figure 4: Network-specific decoding accuracy and compression.** **A. Network parcellation map.** The glass brain displays the location of each of seven networks identified by Yeo et al. (2011). **B. Node labels.** We assigned network labels to each of 700 Hierarchical Topographic Factor Analysis-derived nodes (see *Hierarchical topographic factor analysis (HTFA)*). For each node, we evaluated its radial basis function (RBF) at the locations of every voxel in the parcellation map displayed in Panel A. We summed up these RBF weights separately for the voxels in each network. We defined each node's network label as its highest-weighted network across all voxels. **C. Per-network node counts.** The bar plot displays the total number of HTFA-derived nodes assigned to each network. **D. Informativeness versus compressibility by network and condition.** Each dot corresponds to a single cross validation run. The dots' coordinates denote the minimum proportion of components (relative to the number of nodes in the given network) required to achieve at least 5% corrected decoding accuracy ( $x$ -coordinate; for the rest condition these proportions are estimated using the peak decoding accuracies) and peak (corrected) decoding accuracy ( $y$ -coordinate). We repeated the analysis separately for each network (color) and experimental condition (column). **E. Informativeness by network.** For each network, sorted (roughly) from lower-order networks on the left to higher-order networks on the right, the curves display the peak (corrected) decoding accuracy for each experimental condition (color). **F. Compressibility by network.** For each network, the curves display the proportion of components (relative to the total possible number of components displayed in Panel C) required to achieve at least 5% decoding accuracy (or, for the rest condition, peak decoding accuracy, as described above). Error ribbons in Panels E and F denote bootstrap-estimated 95% confidence intervals.

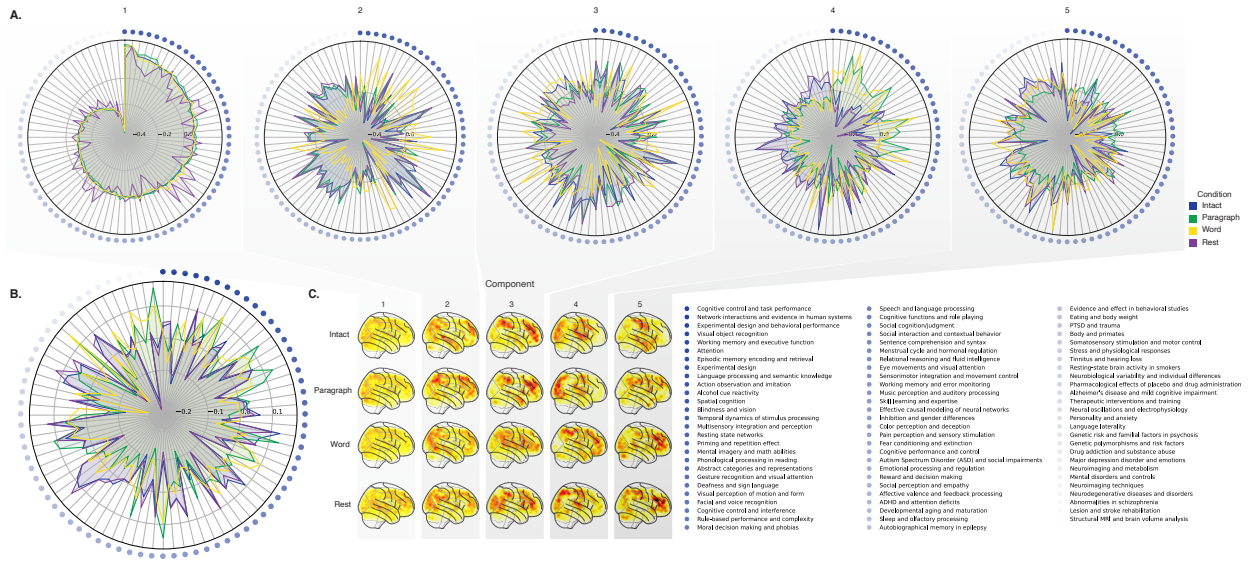


**Figure 5: Neurosynth topic weightings by component.** We used a reverse inference procedure (see *Reverse inference*) to estimate the correspondences between brain images and a set of 80 topics derived from the Neurosynth database of neuroimaging articles (Rubin et al., 2017). **A. Topic correlations by component.** For each of the top five highest-weighted principal components (columns) derived from each experimental condition (colors), the radar plots display the correlations between the component images and the per-topic images derived for each topic (topic identities are denoted by the blue dots; a legend for the topic labels is in the lower right of the figure). An annotated list of the top-weighted topics for each component and condition may be found in Figure S2 and the top-weighted terms for each topic may be found in Table S1. **B. Topic correlations averaged across components.** The radar plot is in the same format as the plots in Panel A, but here we display the per-condition average correlations across the top five components (for each condition) reflected in Panel A. **C. Component images.** Each plot displays a right sagittal view of a glass brain projection of the top five principal components (columns) for each experimental condition (rows). Additional projections for each component may be found in Figure S3.

191 To gain further insights into which brain functions might be most closely associated with  
192 the top-weighted components from each experimental condition, we manually grouped each  
193 Neurosynth-derived topic into a smaller set of core cognitive functions. Separately for each com-  
194 ponent, we computed the average weightings across all topics that were tagged as being associated  
195 with each of these cognitive functions (Figs. 6A, S5A). To help visualize these associations, we used  
196 the patterns of associations for each component to construct graphs whose nodes were experimen-  
197 tal conditions and cognitive functions (Figs. 6B, S5B). We also computed correlations between the  
198 sets of per-topic weightings from each of the top-weighted components from each experimental  
199 condition (Fig. 6C, D) and between the brain maps for each condition's components (Fig. S5C, D).  
200 Taken together, we found that each component appeared to weight on a fundamental set of cogni-  
201 tive functions that varied by experimental condition. For example, the top principal components  
202 from every condition weighted similarly (across conditions) on the full set of Neurosynth topics  
203 (Fig. 5A) and cognitive functions (Figs. 6A, B and S5 A, B), suggesting that these components  
204 might reflect a set of functions or activity patterns that are common across all conditions. The  
205 second components' weightings were similar across the intact, paragraph, and rest conditions  
206 (highest-weighted functions: cognitive control, memory, social cognition, and resting state), but  
207 different for the word condition (highest-weighted functions: sensory perception and cognitive  
208 control). The fourth components' weighting grouped the paragraph and word conditions (highest-  
209 weighted functions: memory, language processing, and cognitive control) and the intact and rest  
210 conditions (highest-weighted functions: emotion, social cognition). We also used ChatGPT (Ope-  
211 nAI, 2023) to sort the list of manually tagged cognitive functions from lowest-level to highest-level  
212 (Tab. S2, Fig. 6E; also see *Ranking cognitive processes*). We found that higher-level functions tended  
213 to be weighted on more heavily by top components from the intact and paragraph conditions  
214 than lower-level functions. The top components from the word condition showed the opposite  
215 tendency, whereby *lower*-level functions tended to be weighted on more heavily than higher-level  
216 functions. The components from the rest condition showed almost no differences in the weights  
217 associated with high-level versus low-level functions.

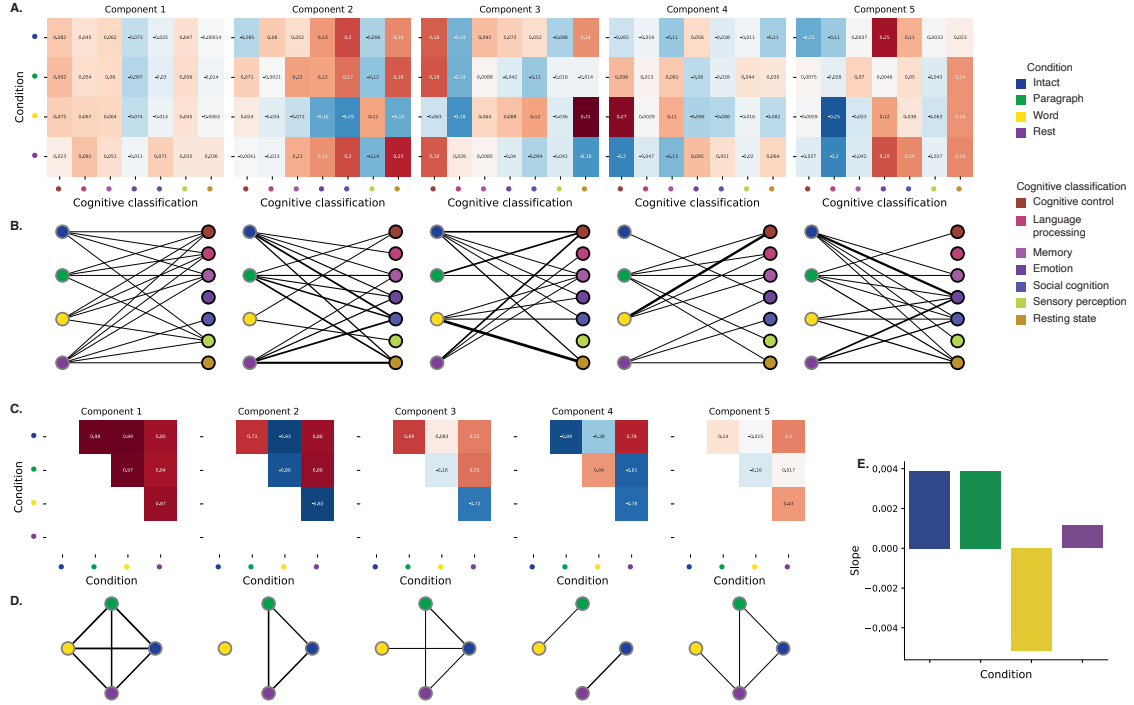


**Figure 6: Summary of functions associated with top-weighted components by condition. A. Top-weighted topics by condition.** Here we display per-condition (rows, indicated by colored dots) topic correlations, averaged across topics that pertain to each of several broad cognitive functions (columns within each sub-panel, indicated by colored dots). Each sub-panel reflects correlations for the components indicated in the panel titles. A legend for the condition and several core cognitive function classifications is displayed in the lower right of the figure. Table S1 provides a list of each topic's top-weighted terms, along with each topic's manually labeled cognitive classification. A full list of the topics most highly associated with each component may be found in Figure S2. **B. Associations between per-condition components and cognitive functions.** The network plots denote positive average correlations between the component images for each condition (gray-outlined dots on the left sides of each network; colors denote conditions) and topic-specific brain maps associated with each indicated cognitive function (black-outlined dots on the right sides of each network; colors denote cognitive functions). The line thicknesses are proportional to the correlation values (correlation coefficients are noted in the heat maps in Panel A). **C. Correlations between each principal component, by condition.** The heat maps display the correlations between the brain maps (Fig. S3) for each principal component (sub-panel), across each pair of conditions (rows and columns of each sub-panel's matrix, indicated by colored dots). **D. Associations between per-condition components, by component.** Each sub-panel's network plot summarizes the pattern of correlations between the  $n^{\text{th}}$  top-weighted principal components (sub-panel) for each experimental condition (gray-outlined dots). The line thicknesses are proportional to the correlation values (correlation coefficients are noted in the heat maps in Panel C). **E. Change in weights by condition.** The bar heights reflect the slopes of regression lines, fit separately to the top five components from each condition, between the ChatGPT-derived "rank" of each cognitive classification and the correlations between the component and topic maps associated with cognitive processes at the given rank (see *Ranking cognitive processes*). Also see Fig. S5 for additional information.

218 **Discussion**

219 We examined fMRI data collected as participants listened to an auditory recording of a story, scram-  
220 bled recordings of the story, or underwent a resting state scan. We found that cognitively richer  
221 stimuli evoked more reliable (i.e., consistent across people) and information rich brain activity pat-  
222 terns. The brain patterns evoked by cognitively richer stimuli were also more compressible, in that  
223 each individual component provided more “signal” to temporal decoders relative to components  
224 of data from less cognitively rich conditions (Fig. 2). Over time (e.g., as the experiment progressed),  
225 these phenomena were strengthened. Specifically, across story segments, data from more cogni-  
226 tively rich conditions became more informative and compressible, and data from less cognitively  
227 rich conditions became *less* informative and compressible (Fig. 3). We also repeated these analyses  
228 separately for different brain networks. We found that networks traditionally associated with  
229 higher-level cognitive functions tended to provide more informative brain patterns than networks  
230 traditionally associated with lower level cognitive functions (Fig. 4). Finally, we examined the most  
231 dominant components of the brain activity patterns from each experimental condition. We used a  
232 reverse inference approach (Rubin et al., 2017) to identify the terms in the neuroimaging literature  
233 most commonly associated with the corresponding maps. As summarized in Figure 6E, we found  
234 that the intact and paragraph conditions tended to weight on higher-level cognitive processes  
235 more than lower-level cognitive processes, whereas the word condition weighted on lower-level  
236 processes more than higher-level processes and the rest condition showed no difference in high-  
237 level versus low-level weighting. Taken together, our findings indicate that the informativeness  
238 and compressibility of our brain activity patterns are task-dependent, and these properties change  
239 systematically with factors like cognitive richness and depth of processing.

240 Our explorations of informativeness and compressibility are related to a much broader litera-  
241 ture on the correlational and causal structure of brain activity patterns and networks (Adachi et  
242 al., 2012; Bassett & Sporns, 2017; Brovelli et al., 2004; Bullmore & Sporns, 2009; Dhamala et al.,  
243 2008; Korzeniewska et al., 2008; Lynn & Bassett, 2021; Owen et al., 2021; Preti et al., 2017; Rogers  
244 et al., 2007; Rubinov & Sporns, 2010; Sizemore et al., 2018; Smith, Beckmann, et al., 2013; Smith,  
245 Vidaurre, et al., 2013; Sporns & Betzel, 2016; Sporns & Honey, 2006; Sporns & Zwi, 2004; Srinivasan  
246 et al., 2007; Tomasi & Volkow, 2011; Yeo et al., 2011). Correlations or causal associations between

247 different brain regions simultaneously imply that full-brain activity patterns will be compressible  
248 and also that those activity patterns will contain redundancies. For example, the extent to which  
249 activity patterns at one brain area can be inferred or predicted from activity patterns at other  
250 areas (e.g., Owen et al., 2020; Scangos et al., 2021), reflects overlap in the information available  
251 in or represented by those brain areas. If brain patterns in one area are recoverable using brain  
252 patterns in another area, then a “signal” used to convey the activity patterns could be compressed  
253 by removing the recoverable activity. Predictable (and therefore redundant) brain activity patterns  
254 are also more robust to signal corruption. For example, even if the activity patterns at one region  
255 are unreadable or unreliable at a given moment, that unreliability could be compensated for by  
256 other regions’ activity patterns that were predictive of the unreliable region.

257 Our findings that informativeness and compressibility change with task demands may follow  
258 from task-dependent changes in full-brain correlation patterns. A number of prior studies have  
259 found that so-called “functional connectivity” (i.e., correlational) patterns vary reliably across  
260 tasks, events, and situations (Cole et al., 2014; Owen et al., 2021; Simony et al., 2016; Smith et  
261 al., 2009). By examining how these task-dependent changes in correlations affect informativeness  
262 and compressibility, our work suggests a potential reason why the statistical structure of brain  
263 activity patterns might vary with cognitive task or with cognitive demands. For lower-level tasks,  
264 or for tasks that require relatively little “deep” cognitive processing, our brains may optimize  
265 activity patterns for robustness and redundancy over expressiveness, for example to maximize  
266 reliability. For higher-level tasks, or for tasks that require deeper cognitive processing, our brains  
267 may sacrifice some redundancy in favor of greater expressiveness.

268 In the information theory sense (Shannon, 1948), when a signal is transmitted using a fixed  
269 alphabet of “symbols,” the information rate decreases as the signal is compressed (e.g., fewer sym-  
270 bols transmitted per unit time, using an alphabet with fewer symbols, etc.). Our finding that each  
271 individual brain component (symbol) becomes more informative as cognitive richness increases  
272 suggests that the “alphabet” of brain activity patterns is also task-dependent. Other work suggests  
273 that the representations that are *reflected* by brain activity patterns may also change with task de-  
274 mands. For example, our brains may represent the same perceptual stimulus differently depending  
275 on which aspects of the stimulus or which combinations of features are task-relevant (Mack et al.,  
276 2020).

277 Different brain networks also varied in how informative and compressible their activity pat-  
278 terns were across experimental conditions (e.g., Fig. 4). This might follow from evolutionary  
279 optimizations that reflect the relevant constraints or demands placed on those networks. One  
280 possibility is that cortex is organized in a hierarchy of networks “concerned with” or selective to  
281 different levels of processing or function. To the extent that different levels of processing (e.g.,  
282 low-level sensory processing versus “deeper” higher-level processing) reflect different stimulus  
283 timescales (e.g., Manning, 2020), the network differences we observed might also relate to the  
284 timescales at which each network is maximally sensitive (Baldassano et al., 2017; Hasson et al.,  
285 2008; Lerner et al., 2011; Regev et al., 2018).

## 286 **Concluding remarks**

287 Cognitive neuroscientists are still grappling with basic questions about the fundamental “rules”  
288 describing how our brains respond, and about how brain activity patterns and the associated  
289 underlying cognitive representations and computations are linked. We identified two aspects of  
290 brain activity patterns, informativeness and compressibility, that appear to change systematically  
291 with task demands and across brain networks. Our work helps to clarify how the “neural code”  
292 might be structured, and how the code might vary across tasks and brain areas.

## 293 **Methods**

294 We measured properties of recorded neuroimaging data under different task conditions that varied  
295 systematically in cognitive engagement and depth of processing. We were especially interested in  
296 how *informative* and *compressible* the activity patterns were under these different conditions (Fig. 1).

### 297 **Functional neuroimaging data collected during story listening**

298 We examined an fMRI dataset collected by Simony et al. (2016) that the authors have made publicly  
299 available at [arks.princeton.edu/ark:/88435/dsp015d86p269k](https://arks.princeton.edu/ark:/88435/dsp015d86p269k). The dataset comprises neuroimaging  
300 data collected as participants listened to an audio recording of a story (intact condition; 36 par-  
301 ticipants), listened to temporally scrambled recordings of the same story (17 participants in the  
302 paragraph-scrambled condition listened to the paragraphs in a randomized order and 36 in the

303 word-scrambled condition listened to the words in a randomized order), or lay resting with their  
304 eyes open in the scanner (rest condition; 36 participants). Full neuroimaging details may be found  
305 in the original paper for which the data were collected (Simony et al., 2016). Procedures were  
306 approved by the Princeton University Committee on Activities Involving Human Subjects, and by  
307 the Western Institutional Review Board (Puyallup, WA). All subjects were native English speakers  
308 with normal hearing and provided written informed consent.

### 309 **Hierarchical topographic factor analysis (HTFA)**

310 Following our prior related work, we used HTFA (Manning et al., 2018) to derive a compact  
311 representation of the neuroimaging data. In brief, this approach approximates the timeseries  
312 of voxel activations (44,415 voxels) using a much smaller number of radial basis function (RBF)  
313 nodes (in this case, 700 nodes, as determined by an optimization procedure; Manning et al., 2018).  
314 This provides a convenient representation for examining full-brain activity patterns and network  
315 dynamics. All of the analyses we carried out on the neuroimaging dataset were performed in  
316 this lower-dimensional space. In other words, each participant's data matrix was a number-of-  
317 timepoints ( $T$ ) by 700 matrix of HTFA-derived factor weights (where the row and column labels  
318 were matched across participants). Code for carrying out HTFA on fMRI data may be found as  
319 part of the BrainIAK toolbox (Capota et al., 2017; Kumar et al., 2021), which may be downloaded  
320 at [brainiak.org](http://brainiak.org).

### 321 **Principal components analysis (PCA)**

322 We applied group PCA (Smith et al., 2014) separately to the HTFA-derived representations of the  
323 data (i.e., factor loadings) from each experimental condition. Specifically, for each condition, we  
324 considered the set of all participants'  $T$  by 700 factor weight matrices. We used group PCA to project  
325 these 700-dimensional matrices into a series of shared  $k$ -dimensional spaces, for  $k \in \{3, 4, 5, \dots, 700\}$ .  
326 This yielded a set of number-of-participants matrices, each with  $T$  rows and  $k$  columns.

327 **Temporal decoding**

328 We sought to identify neural patterns that reflected participants' ongoing cognitive processing of  
329 incoming stimulus information. As reviewed by Simony et al. (2016), one way of homing in on  
330 these stimulus-driven neural patterns is to compare activity patterns across individuals. In partic-  
331 ular, neural patterns will be similar across individuals to the extent that the neural patterns under  
332 consideration are stimulus-driven, and to the extent that the corresponding cognitive representa-  
333 tions are reflected in similar spatial patterns across people (Simony & Chang, 2020). Following this  
334 logic, we used an across-participant temporal decoding test developed by Manning et al. (2018) to  
335 assess the degree to which different neural patterns reflected ongoing stimulus-driven cognitive  
336 processing across people. The approach entails using a subset of the data to train a classifier to  
337 decode stimulus timepoints (i.e., moments in the story participants listened to) from neural pat-  
338 terns. We use decoding (forward inference) accuracy on held-out data, from held-out participants,  
339 as a proxy for the extent to which the inputted neural patterns reflected stimulus-driven cognitive  
340 processing in a similar way across individuals.

341 **Forward inference and decoding accuracy**

342 We used an across-participant correlation-based classifier to decode which stimulus timepoint  
343 matched each timepoint's neural pattern. For a given value of  $k$  (i.e., number of principal compo-  
344 nents), we first used group PCA to project the data from each condition into a shared  $k$ -dimensional  
345 space. Next, we divided the participants into two groups: a template group,  $\mathcal{G}_{\text{template}}$  (i.e., training  
346 data), and a to-be-decoded group,  $\mathcal{G}_{\text{decode}}$  (i.e., test data). We averaged the projected data within  
347 each group to obtain a single  $T$  by  $k$  matrix for each group. Next, we correlated the rows of the two  
348 averaged matrices to form a  $T$  by  $T$  decoding matrix,  $\Lambda$ . In this way, the rows of  $\Lambda$  reflected time-  
349 points from the template group, while the columns reflected timepoints from the to-be-decoded  
350 group. We used  $\Lambda$  to assign temporal labels to each timepoint (row) from the test group's ma-  
351 trix, using the row of the training group's matrix with which it was most highly correlated. We  
352 repeated this decoding procedure, but using  $\mathcal{G}_{\text{decode}}$  as the template group and  $\mathcal{G}_{\text{template}}$  as the  
353 to-be-decoded group. Given the true timepoint labels (for each group), we defined the decoding  
354 accuracy as the average proportion of correctly decoded timepoints, across both groups (where

355 chance performance is  $\frac{1}{T}$ ). In Figures 2 and 3 we report the decoding accuracy for each condition  
356 and value of  $k$ , averaged across  $n = 100$  cross validation folds.

357 **Reverse inference**

358 To help interpret the brain activity patterns we found within the contexts of other studies, we  
359 created summary maps of each principal component, for each experimental condition. Each  
360 principal component comprises 700 “weights” on each of the HTFA-derived RBF nodes (see  
361 *Hierarchical Topographic Factor Analysis*). For each node, we evaluated its RBF at the locations of  
362 every voxel in the standard 2 mm MNI152 template brain and multiplied the RBF by the node’s  
363 weight. The sum of these weighted RBF activation maps provides a full-brain image, in MNI152  
364 space, of the given principal component (Fig. S3).

365 Next, we considered 80 topics estimated using Latent Dirichlet Allocation (Blei et al., 2003)  
366 applied to 9,204 functional neuroimaging articles in the Neurosynth database (Rubin et al., 2017).  
367 The topics, as well as associated brain maps identified using Neurosynth, were identified and  
368 reported in several prior studies (Chen et al., 2020; Fox et al., 2014; Sul et al., 2017). The topic  
369 labels for each topic were generated automatically with the following ChatGPT (OpenAI, 2023)  
370 prompt: “Please help me come up with intuitive labels for topics I found by fitting a topic model  
371 to thousands of neuroscience and psychology articles. I’ll paste in the top 10 highest-weighted  
372 words for each topic, and I’d like you to respond with a suggested label. For each topic, please  
373 respond with just the topic label and no other formatting or text. Here are the next topic’s top  
374 words:” followed by a comma-separated list of the given topic’s top-weighted words reflected  
375 in the Table S1. For some topics, ChatGPT responded with a longer-form response rather than a  
376 concise topic label. In these instances, on a case-by-case basis, we used a second follow-up prompt  
377 to achieve the given topic’s label: “Could you please come up with a more concise label for that  
378 topic?”. We then manually identified a set of 11 cognitive labels that were intended to encapsulate  
379 a representative range of widely studied low-level and high-level cognitive functions. In choosing  
380 the set of cognitive labels, we jointly considered each topic’s ChatGPT-derived topic label, along  
381 with the top-weighted words for the topic. We attempted to generate a concise set of labels that  
382 still spanned the full set of cognitive functions reflected across the 80 topics. Topics that appeared

383 unrelated to specific cognitive functions (e.g., topics related to specific methods or clinical themes)  
384 are designated with dashes in Table S1.

385 Finally, following an approach used in several prior studies (Chen et al., 2020; Fox et al., 2014;  
386 Sul et al., 2017) we treated the correlation between a given component's brain map and each topic's  
387 brain map as an approximate measure of how much the component was reflective of the given  
388 topic. This resulted in a set of 80 "weights" (correlation coefficients) for each component's brain  
389 map, with one weight per Neurosynth-derived topic.

## 390 **Ranking cognitive processes**

391 We manually identified 11 cognitive labels spanning the set of 80 Neurosynth-derived topics:  
392 cognitive control, language processing, memory, emotion, social cognition, spatial cognition, at-  
393 tention, reward, sensory perception, motor control, and resting state. We then used ChatGPT  
394 to automatically "rank" the processes from high-level to low-level using the following prompt:  
395 "Please rank these cognitive processes from highest-level to lowest-level, where higher values  
396 indicate higher-order or higher-level processes. Return the result as a csv file with a header row  
397 and two columns: 'Cognitive label' and 'Rank'. Here are the processes: cognitive control, lan-  
398 guage processing, memory, emotion, social cognition, spatial cognition, attention, reward, sensory  
399 perception, motor control, resting state". Table S2 displays the output. We used these labels  
400 in the analysis presented in Figure 6E to help summarize difference in topic weightings across  
401 experimental conditions.

## 402 **Synthetic data**

403 To help illustrate the relationship between informativeness and compressibility (Fig. 1), we gen-  
404 erated four synthetic datasets, varying in informativeness and compressibility. Each dataset com-  
405 prised simulated observations of  $K = 25$  features across  $N = 100$  timepoints, from each of  $S = 10$   
406 participants. To create each dataset, we first constructed a "template" matrix of  $N$  timepoints by  $K$   
407 features. We then generated participant-specific data by adding independent noise to each entry  
408 in template matrix, drawn from the unit normal distribution (i.e., with a mean of 0 and a variance  
409 of 1). We repeated this process for each participant, yielding  $S$  participant-specific matrices for

410 each dataset.

411 Since we estimate informativeness using the temporal decoding accuracy across participants,  
412 highly informative data will tend to have observations that are highly timepoint specific. Relatively  
413 uninformative data, in contrast, will tend to have more similar observations across timepoints. To  
414 generate data with “high informativeness,” we constructed template matrices whose rows (ob-  
415 servations) were drawn independently from zero-mean multivariate normal distributions. The  
416 covariances of these distributions were determined according to the desired compressibility of  
417 the data, as described below. We used a multi-step process to generate data with “low informa-  
418 tiveness.” First we generated new template matrices using the same procedure as for the “high  
419 informativeness” datasets. We then multiplied each matrix by a constant ( $\rho = 0.1$ ) and computed  
420 the cumulative sum of each matrix’s rows. This yielded matrices whose rows were highly similar  
421 across observations.

422 Compressibility reflects the extent to which decoding accuracy is affected by reducing the num-  
423 ber of components used to represent the data. Highly compressible data will tend to exhibit more  
424 similarities across features, whereas less compressible data will tend to show greater independence  
425 across features. To generate data with “high compressibility,” we set the covariance matrix of the  
426 multivariate normal distribution to a toeplitz matrix whose first row was given by  $[K, K - 1, \dots, 1]$ .  
427 To generate data with “low compressibility,” we set the covariance matrix to the identity matrix.

428 Template matrices for datasets with high informativeness and high compressibility, high in-  
429 formativeness and low compressibility, low informativeness and high compressibility, and low  
430 informativeness and low compressibility are displayed in Figure 1C. The corresponding decoding  
431 curves are displayed in Figure 1D.

## 432 Data and code availability

433 All of the code used to produce the figures and results in this manuscript, along with links to the  
434 corresponding data, may be found at [github.com/ContextLab/pca\\_paper](https://github.com/ContextLab/pca_paper).

435 **Acknowledgements**

436 We acknowledge discussions with Rick Betzel, Luke Chang, Emily Finn, and Jim Haxby. Our  
437 work was supported in part by NSF CAREER Award Number 2145172 to J.R.M. The content is  
438 solely the responsibility of the authors and does not necessarily represent the official views of our  
439 supporting organizations. The funders had no role in study design, data collection and analysis,  
440 decision to publish, or preparation of the manuscript.

441 **Author contributions**

442 Conceptualization: J.R.M. and L.L.W.O. Methodology: J.R.M. and L.L.W.O. Implementation:  
443 J.R.M. and L.L.W.O. Analysis: J.R.M. and L.L.W.O. Writing, Reviewing, and Editing: J.R.M. and  
444 L.L.W.O. Funding acquisition: J.R.M. Supervision: J.R.M.

445 **References**

- 446 Adachi, Y., Osada, T., Sporns, O., Watanabe, T., Matsui, T., Miyamoto, K., & Miyashita, Y.  
447 (2012). Functional connectivity between anatomically unconnected areas is shaped by collective  
448 network-level effects in the macaque cortex. *Cerebral Cortex*, 22(7), 1586–1592.
- 449 Alvarez, S. A. (2002). *An exact analytical relation among recall, precision, and classification accuracy in  
450 information retrieval* (Technical Report No. BCCS-02-01). Boston College.
- 451 Baldassano, C., Chen, J., Zadbood, A., Pillow, J. W., Hasson, U., & Norman, K. A. (2017). Discov-  
452 ering event structure in continuous narrative perception and memory. *Neuron*, 95(3), 709–721.
- 453 Bassett, D. S., & Sporns, O. (2017). Network neuroscience. *Nature Neuroscience*, 20(3), 353–364.
- 454 Blei, D. M., Ng, A. Y., & Jordan, M. I. (2003). Latent dirichlet allocation. *Journal of Machine Learning  
455 Research*, 3, 993–1022.
- 456 Brovelli, A., Ding, M., Ledberg, A., Chen, Y., Nakamura, R., & Bressler, S. (2004). Beta oscillations in  
457 a large-scale sensorimotor cortical network: directional influences revealed by Granger causality.  
458 *Proceedings of the National Academy of Sciences, USA*, 101(26), 9849–9854.

- 459 Bullmore, E., & Sporns, O. (2009). Complex brain networks: graph theoretical analysis of structural  
460 and functional systems. *Nature Reviews Neuroscience*, 10(3), 186–198.
- 461 Capota, M., Turek, J., Chen, P.-H., Zhu, X., Manning, J. R., Sundaram, N., ... Shin, Y. S. (2017).  
462 *Brain imaging analysis kit*.
- 463 Chen, P.-H. A., Jolly, E., Cheong, J. H., & Chang, L. J. (2020). Intersubject representational  
464 similarity analysis reveals individual variations in affective experience when watching erotic  
465 movies. *NeuroImage*, 216(116851), doi.org/10.1016/j.neuroimage.2020.116851.
- 466 Cole, M. W., Bassett, D. S., Power, J. D., Braver, T. S., & Petersen, S. E. (2014). Intrinsic and  
467 task-evoked network architectures of the human brain. *Neuron*, 83(1), 238–251.
- 468 Dhamala, M., Rangarajan, G., & Ding, M. (2008). Analyzing information flow in brain networks  
469 with nonparametric Granger causality. *NeuroImage*, 41(2), 354–362.
- 470 Finn, E. S., Scheinost, D., Finn, D. M., Shen, X., Papademetris, X., & Constable, R. T. (2017).  
471 Can brain state be manipulated to emphasize individual differences in functional connectivity.  
472 *NeuroImage*, 160, 140–151.
- 473 Finn, E. S., Shen, X., Scheinost, D., Rosenberg, M. D., Huang, J., Chun, M. M., ... Constable, R. T.  
474 (2015). Functional connectome fingerprinting: identifying individuals using patterns of brain  
475 connectivity. *Nature Neuroscience*, 18, 1664–1671.
- 476 Fox, A. S., Chang, L. J., Gorgolewski, K. J., & Yarkoni, T. (2014). Bridging psychology and  
477 genetics using large-scale spatial analysis of neuroimaging and neurogenetic data. *bioRxiv*,  
478 doi.org/10.1101/012310.
- 479 Glerean, E., Salmi, J., Lahnakoski, J. M., Jääskeläinen, I. P., & Sams, M. (2012). Functional magnetic  
480 resonance imaging phase synchronization as a measure of dynamic functional connectivity.  
481 *Brain Connectivity*, 2(2), 91–101.
- 482 Gratton, C., Laumann, T. O., Nielsen, A. N., Greene, D. J., Gordon, E. M., Gilmore, A. W., ...  
483 Petersen, S. E. (2018). Functional brain networks are dominated by stable group and individual  
484 factors, not cognitive or daily variation. *Neuron*, 98(2), 439–452.

- 485 Hasson, U., Yang, E., Vallines, I., Heeger, D. J., & Rubin, N. (2008). A hierarchy of temporal  
486 receptive windows in human cortex. *The Journal of Neuroscience*, 28(10), 2539–2550.
- 487 Korzeniewska, A., Crainiceanu, C. M., Kus, R., Franaszczuk, P. J., & Crone, N. E. (2008). Dynamics  
488 of event-related causality in brain electrical activity. *Human Brain Mapping*, 29(10).
- 489 Kumar, M., Anderson, M. J., Antony, J. W., Baldassano, C., Brooks, P. P., Cai, M. B., ... Norman,  
490 K. A. (2021). BrainIAK: the brain image analysis kit. *Aperture*, *In press*.
- 491 Lerner, Y., Honey, C. J., Silbert, L. J., & Hasson, U. (2011). Topographic mapping of a hierarchy of  
492 temporal receptive windows using a narrated story. *The Journal of Neuroscience*, 31(8), 2906–2915.
- 493 Lynn, C. W., & Bassett, D. S. (2021). Quantifying the compressibility of complex networks.  
494 *Proceedings of the National Academy of Sciences, USA*, 118(32), e2023473118.
- 495 Mack, M. L., Preston, A. R., & Love, B. C. (2020). Ventromedial prefrontal cortex compression during  
496 concept learning. *Nature Communications*, 11(46), doi.org/10.1038/s41467-019-13930-8.
- 497 Manning, J. R. (2020). Context reinstatement. In M. J. Kahana & A. D. Wagner (Eds.), *Handbook of  
498 human memory*. Oxford University Press.
- 499 Manning, J. R., Zhu, X., Willke, T. L., Ranganath, R., Stachenfeld, K., Hasson, U., ... Norman,  
500 K. A. (2018). A probabilistic approach to discovering dynamic full-brain functional connectivity patterns.  
501 *NeuroImage*, 180, 243–252.
- 502 Norman, K. A., Polyn, S. M., Detre, G. J., & Haxby, J. V. (2006). Beyond mind-reading: multi-voxel  
503 pattern analysis of fMRI data. *Trends in Cognitive Sciences*, 10(9), 424–430.
- 504 OpenAI. (2023, March). *ChatGPT*. Personal communication.
- 505 Owen, L. L. W., Chang, T. H., & Manning, J. R. (2021). High-level cognition during story listening is  
506 reflected in high-order dynamic correlations in neural activity patterns. *Nature Communications*,  
507 12(5728), doi.org/10.1038/s41467-021-25876-x.
- 508 Owen, L. L. W., Muntianu, T. A., Heusser, A. C., Daly, P., Scangos, K. W., & Manning, J. R. (2020). A  
509 Gaussian process model of human electrocorticographic data. *Cerebral Cortex*, 30(10), 5333–5345.

- 510 Preti, M. G., Bolton, T. A. W., & Van De Ville, D. (2017). The dynamic functional connectome:  
511 state-of-the-art and perspectives. *NeuroImage*, 160, 41–54.
- 512 Regev, M., Simony, E., Lee, K., Tan, K. M., Chen, J., & Hasson, U. (2018). Propagation of information  
513 along the cortical hierarchy as a function of attention while reading and listening to stories.  
514 *Cerebral Cortex*.
- 515 Rogers, B. P., Morgan, V. L., Newton, A. T., & Gore, J. C. (2007). Assessing functional connectivity  
516 in the human brain by fMRI. *Magnetic Resonance Imaging*, 25(11), 1347–1357.
- 517 Rubin, T. N., Kyojo, O., Gorgolewski, K. J., Jones, M. N., Poldrack, R. A., & Yarkoni, T. (2017).  
518 Decoding brain activity using a large-scale probabilistic functional-anatomical atlas of human  
519 cognition. *PLoS Computational Biology*, 13(10), e1005649.
- 520 Rubinov, M., & Sporns, O. (2010). Complex network measures of brain connectivity: uses and  
521 interpretations. *NeuroImage*, 52, 1059–1069.
- 522 Scangos, K. W., Khambhati, A. N., Daly, P. M., Owen, L. L. W., Manning, J. R., Ambrose, J. B.,  
523 ... Chang, E. F. (2021). Biomarkers of depression symptoms defined by direct intracranial  
524 neurophysiology. *Frontiers in Human Neuroscience*, In press.
- 525 Shannon, C. E. (1948). A mathematical theory of communication. *Bell System Technical Journal*,  
526 27(3), 379–423.
- 527 Simony, E., & Chang, C. (2020). Analysis of stimulus-induced brain dynamics during naturalistic  
528 paradigms. *NeuroImage*, 216, 116461.
- 529 Simony, E., Honey, C. J., Chen, J., & Hasson, U. (2016). Dynamic reconfiguration of the default  
530 mode network during narrative comprehension. *Nature Communications*, 7(12141), 1–13.
- 531 Sizemore, A. E., Giusti, C., Kahn, A., Vettel, J. M., Betzel, R. F., & Bassett, D. S. (2018). Cliques and  
532 cavities in the human connectome. *Journal of Computational Neuroscience*, 44(1), 115–145.
- 533 Smith, S. M., Beckmann, C. F., Andersson, J., Auerbach, E. J., Bijsterbosch, J., Douaud, G., ...  
534 Glasser, M. F. (2013). Resting-state fMRI in the Human Connectome Project. *NeuroImage*, 80,  
535 144–168.

- 536 Smith, S. M., Fox, P. T., Miller, K. L., Glahn, D. C., Fox, P. M., Mackay, C. E., ... Beckmann,  
537 C. F. (2009). Correspondence of the brain's functional architecture during activation and rest.  
538 *Proceedings of the National Academy of Sciences, USA*, 106(31), 13040–13045.
- 539 Smith, S. M., Hyvärinen, A., Varoquaux, G., Miller, K. L., & Beckmann, C. F. (2014). Group-PCA  
540 for very large fMRI datasets. *NeuroImage*, 101, 738–749.
- 541 Smith, S. M., Vidaurre, D., Beckmann, C. F., Glasser, M. F., Jenkinson, M., Miller, K. L., ... Van  
542 Essen, D. C. (2013). Functional connectomics from resting-state fMRI. *Trends in Cognitive Sciences*,  
543 17(12), 666–682.
- 544 Sporns, O., & Betzel, R. F. (2016). Modular brain networks. *Annual Review of Psychology*, 67,  
545 613–640.
- 546 Sporns, O., & Honey, C. J. (2006). Small worlds inside big brains. *Proceedings of the National Academy  
of Sciences, USA*, 103(51), 19219–19220.
- 548 Sporns, O., & Zwi, J. D. (2004). The small world of the cerebral cortex. *Neuroinformatics*, 2(2),  
549 145–162.
- 550 Srinivasan, R., Winter, W. R., Ding, J., & Nunez, P. L. (2007). EEG and MEG coherence: Measures of  
551 functional connectivity at distinct spatial scales of neocortical dynamics. *Journal of Neuroscience  
Methods*, 166, 41–52.
- 553 Sul, S., Güroğlu, B., Crone, E. A., & Chang, L. J. (2017). Medial prefrontal cortical thinning  
554 mediates shifts in other-regarding preferences during adolescence. *Scientific Reports*, 7(8510),  
555 doi.org/10.1038/s41598-017-08692-6.
- 556 Tomasi, D., & Volkow, N. D. (2011). Association between functional connectivity hubs and brain  
557 networks. *Cerebral Cortex*, 21, 2003–2013.
- 558 Yeo, B. T. T., Krienen, F. M., Sepulcre, J., Sabuncu, M. R., Lashkari, D., Hollinshead, M., ... Buckner,  
559 R. L. (2011). The organization of the human cerebral cortex estimated by intrinsic functional  
560 connectivity. *Journal of Neurophysiology*, 106(3), 1125–1165.